CRYSTALLIZATION OF $YAlO_3$ PEROVSKITE USING MICROWAVE HYDROTHERMAL TECHNIQUE*

Nikola Cichocka[a,†], Serhiy Kobyakov[a], Jarosław Kaszewski[b]
Roman Minikayev[b], Bartłomiej Witkowski[b], Agata Kamińska[a,b]

[a]Cardinal Stefan Wyszyński University
Faculty of Mathematics and Natural Sciences
School of Exact Sciences, Dewajtis 5, 01-815 Warsaw, Poland
[b]Institute of Physics, Polish Academy of Sciences
Al. Lotników 32/46, 02-668 Warsaw, Poland

(Received May 18, 2020)

Perovskites, garnets, monoclinic forms, and lately also oxyhydroxides doped with rare earth ions have drawn large attention due to their beneficial photovoltaic properties. In this work, ceramic nanopowders of YAP doped with europium were synthesized using microwave-driven hydrothermal technique with different pH and post-growth treatment. The structure as well as optical properties of the materials were investigated as a function of hydrothermal crystallization conditions. For this purpose, the X-ray diffraction, scanning electron microscopy, and the photoluminescence studies of these materials were performed. Optical properties of the nanoparticles in relation with their structure and chemical composition are discussed.

DOI:10.5506/APhysPolBSupp.13.851

1. Introduction

Ceramic crystal powders with nanometric sizes have enjoyed great popularity for many decades. Rare earth doped ceramic powders are used nowadays and can find new applications in industry and medicine [1].

Three crystal types are well-known in the yttrium oxide–alumina system: $YAlO_3$ (YAP), $Y_4Al_2O_9$ (YAM), $Y_3Al_5O_{12}$ (YAG) [2]. These materials are promising for many applications, in particular in optics and electronics.

The most popular ceramic material is cubic yttrium–aluminum garnet ($Y_3Al_5O_{12}$, YAG) [3]. YAG can be easily doped with rare earth ions owing to its crystalline structure. Such materials have a wide spectrum of applications

* Presented at the 45$^{\text{th}}$ Congress of Polish Physicists, Kraków, September 13–18, 2019.

† Corresponding author: ncichocka92@gmail.com

in optoelectronics [4]. Doped YAG nanopowders are used in medicine to destroy cancer cells [5].

Monoclinic $Y_4Al_2O_9$, in addition to applications in optics and electronics, found its application as a thermal barrier due to the very low thermal conductivity [6].

Orthorombic $YAlO_3$ (YAP), often doped with rare-earth ions, can be used as an active element in lasers [7]. This form of perovskite, doped with transition metals shows good luminescence efficiency [8]. YAP doped with alkaline earth ions shows strong photoluminescence (PL) in the visible range of the spectrum when exposed to ultraviolet (UV) radiation [9]. YAP is also an attractive material in optoelectronic applications.

Crystal field symmetry affects spectral properties of Eu^{3+} ions, therefore, they are known as local symmetry sensors [10]. Optical properties shown by the obtained nanoparticles in correlation with their structure and chemical composition have been discussed in several papers [11, 12].

Considering the growing use of nanomaterials, more research on quick, cheap and relativly simple methods of their production is being conducted. Many methods of obtaining nanomaterials require high vacuum, very high temperature and high purity of reagents [13]. Taking this into consideration, the microwave-driven hydrothermal method is a very promising way of yttrium aluminum oxide nanopowders production. This method is not relatively time-consuming in reaction mixture preparation. The reactor is cheap, energy-saving [14] and nanomaterials can be fairly easily doped with rare earth [15].

2. Experimental methods

$Y(NO_3)_3 \cdot 6H_2O$ and $Al(NO_3)_3 \cdot 9H_2O$ were used as a source of yttrium and aluminum in the reaction mixture. Solution of $Eu(NO_3)_3 \cdot 5H_2O$ with distilled water was introduced into the synthesis in order to introduce europium ions. The pH of the solution was equal to 3. Then, 10 M solution of NaOH was added using pipette to reach pH 6 and 8. The pH value was checked using the universal indicator paper. The hydrothermal synthesis was carried out using Magnum Ertec II hydrothermal reactor at 60 bar for 20 minutes for each sample. The temperature has been varied depending on the pressure in reactor, ranging from 150 to 300°C. Later, the product of reaction was calcined at 1200°C for 2 hours at atmospheric pressure in the air.

The X-ray diffraction (XRD) measurements have been used to characterize the crystallographic structure. A suitable set of refined parameters corresponding to measurements conditions, crystallographic parameters (space group and unit cell parameters) of refined phases and modelling pattern

(peak profile, peak asymmetry) were applied. Crystallographic characterization was made by Le Bail method with the help of Fullprof.2k program [16]. The measurements were carried out at X'Pert Pro Alpha1 MPD, Panalytical, a laboratory diffractometer equipped with a primary beam Ge (111) monochromator and position-sensitive linear semiconductor detector (X'Celerator). The Cu X-ray tube was applied.

The high resolution (1 nm) scanning electron microscopy (SEM) Hitachi SU-70 has been used to characterize the morphology and properties of the grown samples. The microscope had two secondary electron detectors (SE) and a backscattered electron detector (BSE) that allowed to visualize the atomic contrast and material density differences with remarkable sensitivity. The nanopowders were applied to silicon wafers using water in order to produce SEM images.

The photoluminescence emission (PL) and excitation (PLE) spectra were measured at the room temperature using Horiba/Jobin-Yvon Fluorolog-3 spectrofluorometer equipped with a continuous Xe lamp as an excitation source and Hamamatsu 928P PMT detector (250–850 nm) in photon counting mode. All spectra were corrected for the excitation spectral intensity using photodiode.

3. Experimental results

3.1. X-ray diffraction

XRD patterns are presented in figure 1 for (a) samples as crystallized in the microwave hydrothermal process and (b) calcined at 1200°C for 2 hours. The phase composition of the samples depends on the pH value used in the preparation. At pH 3, obtained product is an anorthic form of $Y(NO_3)_3 \cdot 5H_2O$ (pdf card No. 75-2104), all the reflexes on the diffraction pattern are attributed to this phase. Synthesis at pH 6 and 8 resulted in crystallization of m-$Y_4O(OH)_9(NO_3)$ (pdf card No. 79-1352) mixtures with r-$NaNO_3$ (01-0840) and o-AlO(OH) (21-1307). Monoclinic $Y_4O(OH)_9(NO_3)$ phase dominates in both samples, however, its quantity is the highest at pH 8 (63%). After calcination in the sample prepared at pH 3, one can find mainly orthorhombic $YAlO_3$ (perovskite type) phase (pdf card No. 08-0147), cubic $Y_3Al_5O_{12}$ (YAG, pdf card No. 33-0040), monoclinic $Y_4Al_2O_9$ (YAM, pdf card No. 34-0368) and cubic Y_2O_3 (pdf card No. 41-1105). Quantitatively, the perovskite phase dominates (46%), next there are YAG (37%), YAM (14%) and Y_2O_3 (2%). In pH 6 and 8 synthesized and then calcined samples, there is a mixture of c-Y_2O_3 (41-1105), m-$Al_2Y_4O_9$ (34-0368), c-$Al_5Y_3O_{12}$ (33-0040) and r-$Na_{1.7}Al_{11}O_{17}$ (84-0381).

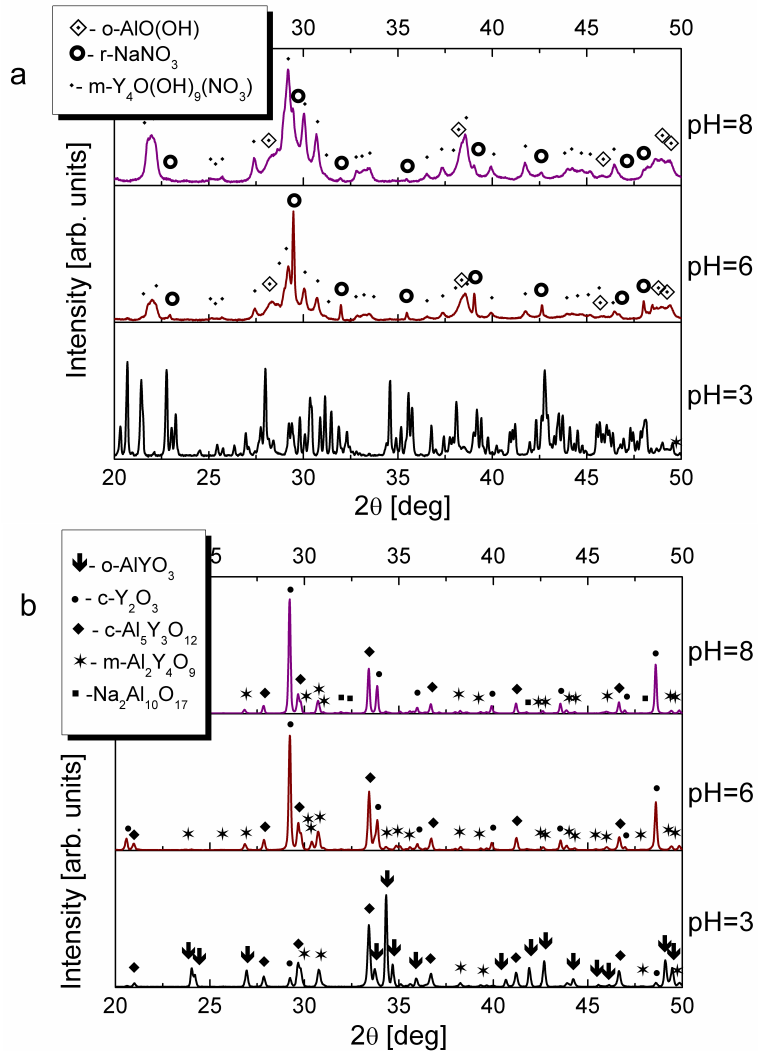

Fig. 1. XRD patterns of samples prepared at pH values of 3, 6 and 8 in microwave hydrothermal process (a) and additionally calcined at 1200°C (b).

3.2. Scanning electron microscopy

Morphology of powders is presented in figures 2, 3 and 4. Comparing figures 2, 3 and 4, sintering of agglomerates at 1200°C is visible. Comparing figures 2 and 3 with pH value 6 and 8, it can be concluded that a larger sintering occurs as the amount of $Y_4O(OH)_9(NO_3)$ and AlO(OH) increases, as it was observed previously in [13].

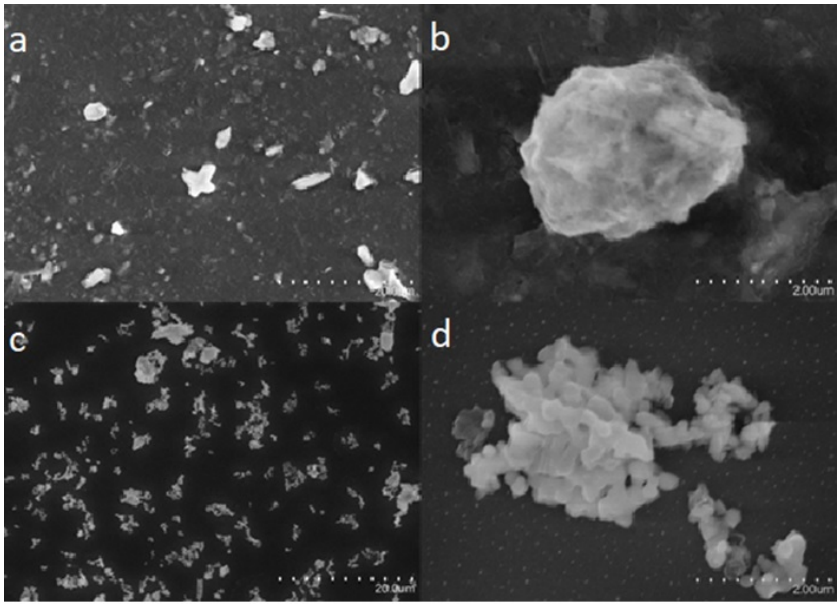

Fig. 2. Morphology of samples obtained by hydrothermal method at pH 8 as-grown (a), (b) and 1200°C calcined (c), (d).

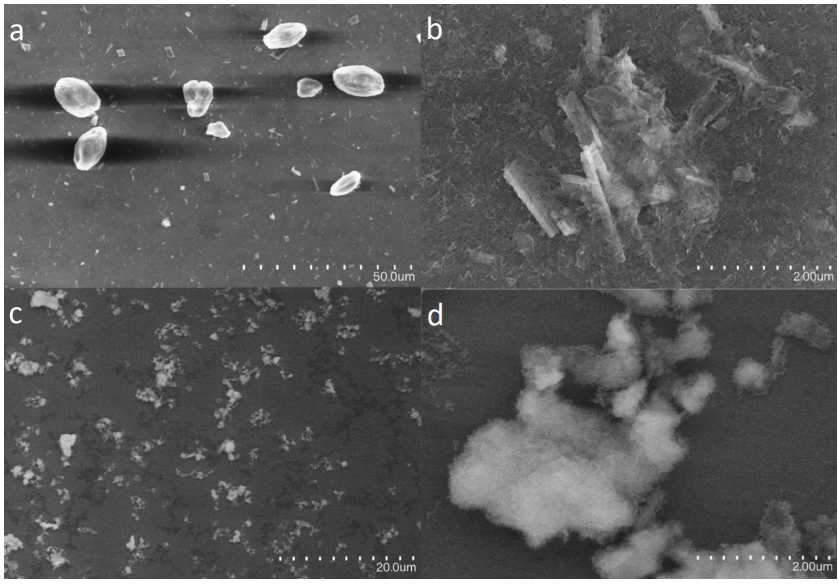

Fig. 3. Morphology of samples obtained by hydrothermal method at pH 6 as-grown (a), (b) and 1200°C calcined (c), (d).

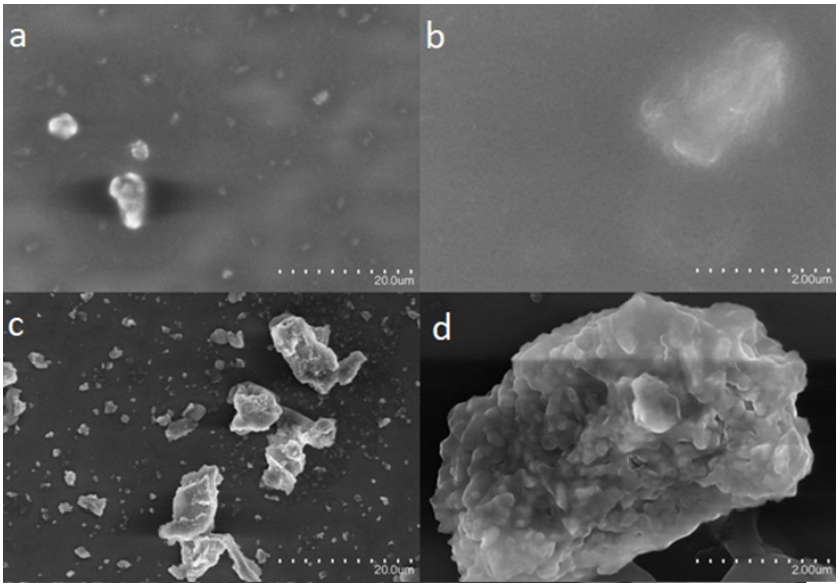

Fig. 4. Morphology of samples obtained by hydrothermal method at pH 3 as-grown (a), (b) and 1200°C calcined (c), (d).

3.3. Spectroscopic properties

Figure 5 shows emission spectra of the as-grown and calcined at 1200°C powders. The different $^5D_0 \rightarrow {}^7F_J$ transitions of Eu^{3+} are visible. The strongest emission is observed for $J = 2$ for as-grown samples (at 617 nm). There are emission peaks at 590 nm (transition $^5D_0 \rightarrow {}^7F_1$), 617 nm ($^5D_0 \rightarrow {}^7F_2$), 649 nm ($^5D_0 \rightarrow {}^7F_3$) and at 710 nm ($^5D_0 \rightarrow {}^7F_4$). An intense transition at 617 nm is a sign of strong crystal-field perturbation [10]. For sample as-grown at pH 3 lines at 590 nm and 617 nm (Fig. 5 a) are related to electric and magnetic dipole f–f transitions [10].

For calcined samples, there are two intensive emission lines at 590 nm ($^5D_0 \rightarrow {}^7F_1$) and at 710 nm ($^5D_0 \rightarrow {}^7F_4$). The $^5D_0 \rightarrow {}^7F_1$ is a magnetic dipole (MD) transition [10, 17].

Annealed samples show comparable intensities of emission spectra (Fig. 5 (b)). The spectra contain several lines between 580 nm and 720 nm with the most intense $^5D_0 \rightarrow {}^7F_1$ transition (590 nm) and $^5D_0 \rightarrow {}^7F_4$ transition (710 nm). For all annealed samples, the $^5D_0 \rightarrow {}^7F_1$ and $^5D_0 \rightarrow {}^7F_4$ transitions are of the highest intensity. The $^5D_0 \rightarrow {}^7F_4$ transition is explained by a highly polarisable chemical environment, which suggests a local symmetry corresponding to a slightly distorted coordination geometry [10, 18].

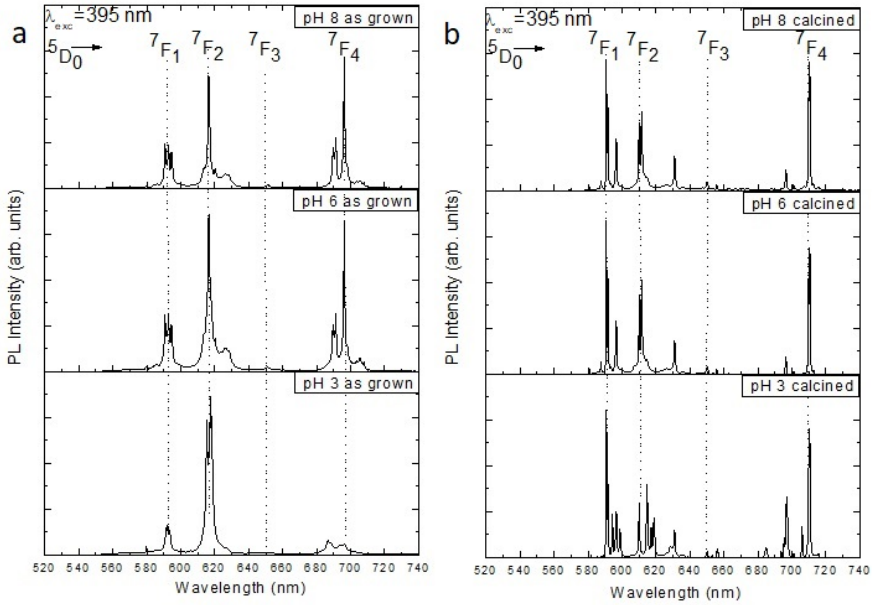

Fig. 5. PL spectra of samples obtained by the hydrothermal method as-grown (a), 1200°C calcined (b) ($\lambda_{exc} = 395$ nm, room temperature).

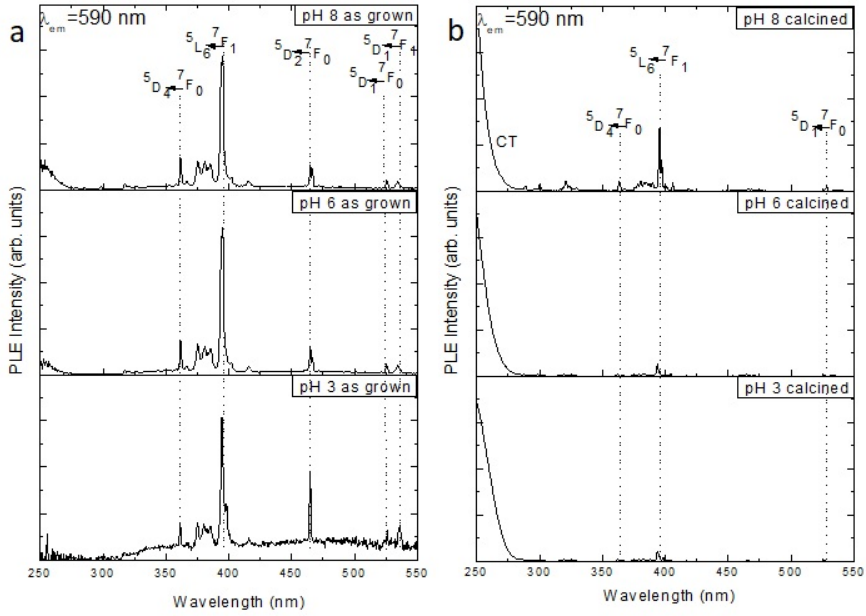

Fig. 6. PLE spectra of samples obtained by the hydrothermal method as-grown (a), 1200°C calcined (b) ($\lambda_{em} = 590$ nm, room temperature).

Figure 6 presents excitation spectra for all samples at emission wavelength 590 nm. The most intense $^5L_6 \leftarrow {}^7F_1$ transition is clearly visible. The calcined samples reveal a broad absorption band in the ultraviolet region, which is due to the charge-transfer (CT) process [10]. This is caused by the transfer of electron from the ligand O^{2-} $(2p^6)$ orbitals to the empty states of $4f^6$ for Eu^{3+} configuration [10].

4. Discussion

Figure 1 shows the XRD patterns for powders obtained by hydrothermal method. Analyzing the XRD results, it can be concluded that compounds $Y_4O(OH)_9(NO_3)$ and $Y(NO_3)_3 \cdot 5H_2O$ are mainly responsible for the formation of $YAlO_3$ and Y_2O_3.

Figures 2, 3, and 4 show SEM images obtained for samples synthesized by hydrothermal method. It can be seen that after calcination, the structure of powder is granular with a number of individual grains sticking very close to each other, resulting in the formation of irregularly shaped agglomerates. The size of the agglomerates is widely distributed. Powders obtained by hydrothermal as-grown method are much smaller. Addition of NaOH results in larger structures. The dependence of composition and grain sizes of obtained material on pH of reaction mixture and post-growth treatment is summarized in figure 7.

as grown

pH	3	6	8
grain sizes	0,2 - 1,5 µm	0,2 - 5 µm	1 - 5 µm
predominant phases	$Y(NO_3)_3{\cdot}5H_2O$	$Y_4O(OH)_9(NO_3)$ $NaNO_3$	$Y_4O(OH)_9(NO_3)$ $AlO(OH)$

calcined

pH	3	6	8
grain sizes	0,2 - 6 µm	2 - 6 µm	4 - 10 µm
predominant phases	$YAlO_3$ $Y_3Al_5O_{12}$	$Y_3Al_5O_{12}$ Y_2O_3	Y_2O_3 $Y_3Al_5O_{12}$

Fig. 7. The dependence of composition and grain sizes of obtained material on pH of reaction mixture and post-growth treatment.

For the annealed samples, the $^5D_0 \rightarrow {}^7F_1$ transition is of highest intensity, which indicates that Eu^{3+} ions have centro-symmetrical environment in structure [10]. The PL spectra of as-grown samples also show the same three emission lines, but with different relative intensities, the $^5D_0 \rightarrow {}^7F_2$

transition is the most prominent one. The PL spectrum of the as-grown sample at pH 3 does not show $^5D_0 \rightarrow {}^7F_4$ transition, which means that Eu^{3+} does not incorporate in centro-symmetrical environment at these conditions [10, 19]. Comparing the transition intensity in the spectra and the symmetry of Eu^{3+} ion surrounding deduced from PL properties, it can be stated that $YAlO_3$:Eu is present in the annealed samples.

As-grown samples show no charge transfer band in comparison to annealed ones, which is due to their different excitation mechanisms. The $^5L_6 \leftarrow {}^7F_1$ transition is the most intense in excitation spectrum of Eu^{3+}, therefore, the ligand excitation is not possible owing to low efficiency of energy transfer [10]. CT energy depends on electron affinity, distance of the metal from the ligand and electronegativity. For calcined powder crystals, $^5L_6 \leftarrow {}^7F_1$, $^5D_2 \leftarrow {}^7F_0$, $^5D_1 \leftarrow {}^7F_0$ transitions are much less intensive comparing with the as-grown samples.

5. Conclusions

YAP, YAG and YAM were obtained using hydrothermal method with different pH of reaction mixture, after annealing at 1200°C. The composition of the obtained nanopowder depends on pH of reaction mixture showing the decrease of perovskite $YAlO_3$ phase content with increasing pH. Further work is necessary to optimize growing conditions in order to increase useful phase outcome.

REFERENCES

[1] F. Iskandar, *Adv. Powder Technol.* **20**, 283 (2009).
[2] I. Warshaw *et al.*, *J. Am. Ceram. Soc.* **42**, 434 (1959).
[3] A. Ikesue *et al.*, *J. Am. Ceram. Soc.* **78**, 225 (1995).
[4] B. Cockayne *et al.*, *J. Less Common Met.* **114**, 199 (1985).
[5] I. Kaminska *et al.*, presented at the Biomolecules and Nanostructures 4 Conference, Pułtusk, Poland, 15–19 May, 2013.
[6] Y. Zhou *et al.*, *J. Adv. Ceram.* **4**, 94 (2015).
[7] M.J. Weber, *J. Appl. Phys.* **44**, 3205 (1973).
[8] A. Phunpueok *et al.*, *Nucl. Instrum. Methods Phys. Res. B* **286**, 76 (2012).
[9] Y. Kawab *et al.*, *J. Lumin.* **121**, 517 (2006).
[10] K. Binnemans, *Coordin. Chem. Rev.* **295**, 1 (2015).
[11] D. Hreniak *et al.*, *J. Alloys Compd.* **408-412**, 828 (2006).
[12] P. Tanner *et al.*, *J. Alloys Compd.* **424**, 347 (2006).
[13] Yu. Zorenko *et al.*, *Radiat. Meas.* **45**, 395 (2010).

[14] Safety data sheet of Magnum Ertec II Reactor, http://www.ertec.pl/pl/oferta/mineralizatory/11-magnum-v2, accessed: 08.2019.

[15] K. Byrappa, T. Adschiri, *Prog. Cryst. Grow. Charact. Matter.* **53**, 117 (2017).

[16] J. Rodríguez-Carvajal, *Newsletter in Commission on Powder Diffraction (IUCr)* **26**, 12 (2001).

[17] M. Mitsunaga, N. Uesugi, *J. Lumin.* **48–49**, 459 (1991).

[18] R.A. Sá Ferreira *et al.*, *J. Lumin.* **121**, 561 (2006).

[19] H. Forest *et al.*, *J. Am. Chem. Soc.* **133**, 15475 (2011).